Research Square

Preprints are preliminary reports that have not undergone peer review.
They should not be considered conclusive, used to inform clinical practice,
or referenced by the media as validated information.

Unified Creep Model for Geological Hazards with Endogenous-Exogenous Coupling Mechanism

Biao Wang

Wangbiao09100710@163.com

China Three Gorges University

Qingjun ZUO

China Three Gorges University

maolin Deng

China Three Gorges University

Qinglin Yi

China Three Gorges University

Physical Sciences - Article

Keywords:

Posted Date: March 13th, 2026

DOI: https://doi.org/10.21203/rs.3.rs-9093798/v1

License: This work is licensed under a Creative Commons Attribution 4.0 International License.
Read Full License

Additional Declarations: There is **NO** Competing Interest.

Title: Unified Creep Model for Geological Hazards with Endogenous-Exogenous Coupling Mechanism

Author list:

Biao Wang [1,2*], Qingjun Zuo [1,2*], Maolin Deng [1,2*], Qinglin Yi [1,2]

Affiliations:

1. National Field Observation and Research Station of Landslides in Three Gorges Reservoir Area of Yangtze River, China Three Gorges University, Yichang, Hubei 443002, China;

2. College of Civil Engineering & Architecture, China Three Gorges University, Yichang, Hubei 443002, China;

Abstract

Geological hazards are not isolated events within the Earth system; rather, they exhibit complex interactions that can trigger cascading effects[1]. Revealing the coupling mechanisms between endogenous damage-healing processes and exogenous loading, and clarifying their dominant roles at different creep stages, has become an urgent priority in hazard prediction research. Based on the power-law relationship between displacement and rate, we propose a unified creep model for geological hazards: $\dot{\Omega}(t)=A(t)\Omega^{n(t)}$, where Ω represents displacement or strain, $A(t)$ is the endogenous damage parameter, and $n(t)$ denotes the exogenous loading parameter. This model comprehensively describes the deceleration, steady-state, and acceleration stages of creep and is applicable to various geological hazards such as landslides, volcanic eruptions, rock bursts, glacier movements, and fault slips. Furthermore, it can be extended to engineering materials, including metal alloys, polymers, and asphalt concrete. Through mathematical transformation, this model unifies the Voight, Saito, Andrade, and Monkman-Grant creep models[2-5], revealing the power-law dynamics shared by both geological and engineering materials. Based on the analytical solution of the model, we discovered a linear relationship between $\Omega^{(1-n)}$ and the remaining time to failure t_f-t, thereby establishing a novel method for predicting creep and failure time that has been validated across multiple disaster scenarios. Furthermore, we established an endogenous-exogenous A-n coupling analysis framework to elucidate the dominant factors influencing each stage of creep deformation. This framework systematically deciphers the damage-healing-relocking process of fault zones under earthquake disturbances, as well

as the disaster mechanisms associated with the slow sliding of giant rock landslides, volcanic flank collapses, and glacial slips. The model not only functions as a practical tool for hazard prediction but also clarifies the interactions among multiple hazards, thereby providing a theoretical foundation for understanding the complex cascade effects of disasters within the Earth system.

Introduction

Geological hazards, including catastrophic landslides, volcanic eruptions, earthquakes, and glacier collapses, pose significant threats to human society. Understanding their deformation mechanisms and developing effective creep prediction methods are core research objectives in fields such as geomechanics, seismology, glaciology, and engineering sciences[6-7]. Despite advancements in high-precision monitoring technologies that have generated vast amounts of observational data, accurately predicting hazards remains a formidable challenge. This challenge arises from the highly heterogeneous nature of geological materials, the complexity of hazard-triggering mechanisms, and our limited understanding of the full life-cycle creep behavior of these materials, as well as their endogenous and exogenous driving mechanisms[8-9].

Fukuzono and Voight revealed a power-law relationship between acceleration and rate during the terminal creep stage, laying the groundwork for predicting disasters such as landslides and volcanic eruptions[2,10-11]. The log-periodic power law singularity (LPPLS) model proposed by Lei et al. characterizes the oscillatory behavior of materials as they accelerate and decelerate prior to failure[6]. From the perspective of endogenous-exogenous interaction, it elucidates the coupling mechanism between exogenous stresses, such as rainfall, and the endogenous damage-healing process[12]. However, existing models generally lack universality across different materials and creep stages; most focus solely on the final accelerated creep stages, neglecting critical information embedded in the deceleration and steady-state creep stages. Furthermore, the parameters of these models often lack clear physical significance, making it challenging to establish direct correlations with endogenous damage evolution or exogenous loads, and to clarify the dominant roles and coupling mechanisms of endogenous and exogenous factors during various disaster incubation stages.

The initiation and occurrence of disasters are fundamentally driven by the interplay between the intrinsic stability of geological bodies (endogenous factors) and external loads (exogenous factors). Endogenous factors primarily involve the accumulation and healing of internal material damage, such as shear slip and crack propagation, while exogenous factors encompass environmental disturbances,

including rainfall, earthquakes, and fluctuations in reservoir water levels[13]. Whether their interaction constitutes a unidirectional influence, bidirectional feedback, or an inseparable coupled process remains unclear, with the complex mechanisms still not fully understood[14-15]. Phenomena such as elevated pore fluid pressure can act as both external disturbances and triggers for internal strength degradation. These coupling effects play a critical role in landslides, fault reactivation, and volcanic flank collapse[16-17]. Therefore, establishing a physical model that can uniformly describe full-stage creep behavior while characterizing endogenous-exogenous coupling mechanisms has become an urgent requirement in contemporary hazard prediction research.

To address this issue, we propose a unified creep model for geological hazards based on an endogenous-exogenous coupling mechanism, represented as $\dot{\Omega}(t)=A(t)\Omega^{n(t)}$. Through derivation, we obtain analytical solutions for both rate and displacement, revealing a linear relationship between $\Omega^{(1-n)}$ and the remaining time to failure, t_f-t. Building on this foundation, we establish a novel method for predicting creep behavior and failure time, which has been validated across various geological hazard cases. This model integrates multiple creep models, including Voight, Saito, Andrade, and Monkman-Grant, into a single theoretical framework[2-5], thereby establishing a universal theoretical correlation for cross-material creep prediction.

By analyzing five consecutive creep events of the Tanjiawan landslide in the Three Gorges Reservoir area (TGRA), we elucidated the coupling mechanism between endogenous damage-healing processes and exogenous loading by examining the variation patterns of the endogenous damage parameter A and the exogenous load parameter n. Exogenous events, such as earthquakes and extreme rainfall, can trigger initial disasters by increasing the value of n. Concurrently, post-disaster structural damage to geological bodies modifies their susceptibility to subsequent disturbances, leading to cascading disasters. For instance, earthquake-induced landslides not only cause direct destruction but also degrade mountain materials, significantly heightening the risk of subsequent rainfall-triggered debris flows. Similarly, the interaction between long-term magmatic activity (endogenous degradation) on volcanic flanks and short-term seismic disturbances (exogenous triggering) is a critical factor contributing to volcanic collapse and triggering compound disaster chains, such as tsunamis[17-18]. Therefore, the creep model we propose not only serves as a practical tool for disaster prediction but also establishes a theoretical foundation for elucidating interactions among multiple hazards and

clarifying complex disaster cascades in Earth systems through the construction of an endogenous-exogenous A-n coupling analysis framework.

Unified Creep Model for Geological Hazards.

We propose a unified creep model (Equation 1) that achieves comprehensive coverage across all stages by employing time-varying parameters. This model provides a novel theoretical framework for the unified description and prediction of material creep. Each parameter within the model possesses distinct physical significance: Ω represents directly observable physical quantities such as displacement and strain; $\dot{\Omega}$ denotes the creep rate; $A(t)$ is the endogenous damage parameter, and $n(t)$ represents the exogenous loading parameter.

$$\dot{\Omega}(t)=A(t)\Omega^{n(t)} \tag{1}$$

When the system is in motion ($\dot{\Omega} > 0$), the Ω value remains positive, irrespective of whether it is in deceleration creep, constant creep, or accelerated creep. Consequently, a logarithmic transformation can be safely applied to establish a linear relationship, facilitating unified fitting across the entire creep process.

$$log\dot{\Omega}=logA+nlog\Omega \tag{2}$$

We validated the universality of this model through various material examples (Fig. 1), including landslides, volcanic eruptions, rockbursts, glacier movements, fault slips, metal alloys, polymers, and asphalt concrete. The data generally exhibit significant linear relationships in the $log\dot{\Omega}-log\Omega$ plot ($R^2>0.9$, $p<0.001$), indicating that despite the differing creep modes of these materials, their rate-displacement evolution adheres to a common power-law pattern.

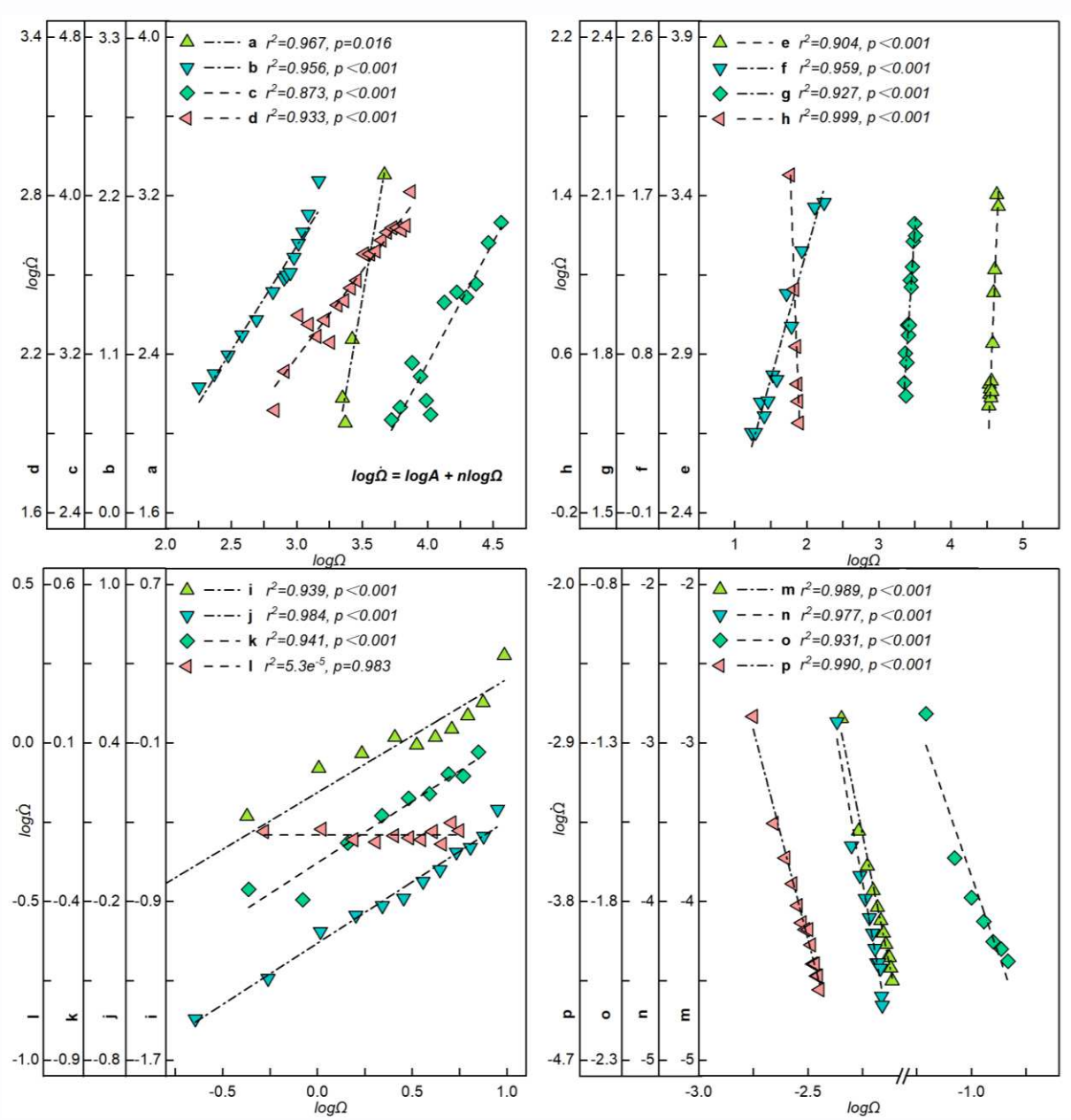


Fig.1 The relationship between rate and displacement following a power-law in the deceleration creep, constant creep, and accelerated creep stages is analyzed for various events, each associated with a specific meaning of Ω. *a*, Xintan landslide, China[19], Ω=surface displacement (mm), A=3.105×10^{-11}, n=3.768, accelerating failure during Mar-Jun 1985; *b*, Vaiont landslide, Italy[20], Ω=surface displacement (mm), A=0.003, n=1.457, accelerating failure on Oct 9, 1963; *c*, La Clapière landslides, Ω=surface displacement (mm), A=0.018, n=1.223, accelerating failure during 1982-1987; *d*, Achoma Landslide, Peru[21], Ω=surface displacement (mm), A=1.663, n=0.656, accelerating failure during Apr-Jun 18, 2020; *e*, Glacier at Grandes Jorasses, Italy[6], Ω=surface displacement (mm), A=3.05×10^{-23}, n=5.564, accelerating prior to ice breakoff on Sep 23; *f*, rockburst at New South Wales, Australia[6], Ω=tunnel roof displacement (mm), A=0.03, n=1.457, accelerating prior to rockburst; *g*, volcanic eruption at Axial Seamount, Pacific Ocean[6], Ω=seafloor uplift (mm), A=6.067×10^{-6}, n=2.072, accelerating prior to eruption in Apr 2011; *h*, Nippes earthquake, 2021, Ω=slip (mm), A=2.168×10^{19},

n=-10.059, postseismic aseismic slip on Enriquillo Plantain Garden Fault[22]; *i-j-k-l*, UNS N10003 alloy at 650℃, Ω=strain, A=0.439~0.527, n=0~0.573, creep under 250MPa, 275MPa, 320MPa, 380MPa respectively[23]; *m*, Ti-6Al alloy[4], Ω=strain, A=8.59×10^{-19}, n=-6.661, creep at 716MPa; *n*, Ti-6242 alloy[4], Ω=strain, A=1.875×10^{-21}, n=-7.711, creep at 931MPa; *o*, tested TSL (thin spray-on liner), Ω=strain, A=1.972×10^{-4}, n=-1.984, creep with different curing times[24]; *p*, HMAC (high-modulus asphalt concrete) pavement, Ω=strain, A=1.2×10^{-16}, n=-4.763, creep[25].

Parameter evolution and physical implications

The Tanjiawan landslide is located on the right bank of the Zhaxi River, a tributary of the Yangtze River (110°40′27.3″ E, 31°04′16.4″ N), and is characterized by an average slope of 27°. The landslide body extends 450 m in length and has an average thickness of approximately 20 m, resulting in a total volume of 3.15 million m^3. The landslide mass primarily consists of gravelly soil, while the sliding bed is composed of interbedded Jurassic sandstone and mudstone bedrock (Fig. 2). Following the impoundment of the Three Gorges Reservoir to a height of 175 m in 2008, the reservoir water level has exhibited significant fluctuations between 145 m and 175 m annually. This variability, combined with heavy rainfall, has emerged as a major triggering factor for geological disasters in Zigui County. This study analyzes data from the fully automated GNSS displacement monitoring point G11 and the groundwater level monitoring point S1 during five creep processes (Stages A to E) of the landslide from May to December 2020.

The time-varying characteristics of model parameters exhibit a clear correspondence with the creep stages of geological materials (Fig. 3). During the steady-state creep stage, the logarithmic variation amplitude of the creep rate is minimal, as evidenced by the $log\dot{\Omega}$–$log\Omega$ plot, which presents a horizontal line with a slope approaching zero. In the accelerated creep stage, $log\dot{\Omega}$ increases significantly with $log\Omega$, resulting in a slope greater than one (n>1). Conversely, during the decelerated creep stage, $log\dot{\Omega}$ decreases with increasing $log\Omega$, corresponding to a slope of n < 1. The period from days 39 to 43 is characterized by accelerated creep, while days 44 to 65 indicate a transition to the decelerated creep stage, with n(t) < 0. This cycle closely aligns with the five creep cycles driven by rainfall-induced groundwater level rise. Furthermore, following the creep events on days 25 and 65, both A(t) and n(t) revert to their initial states.

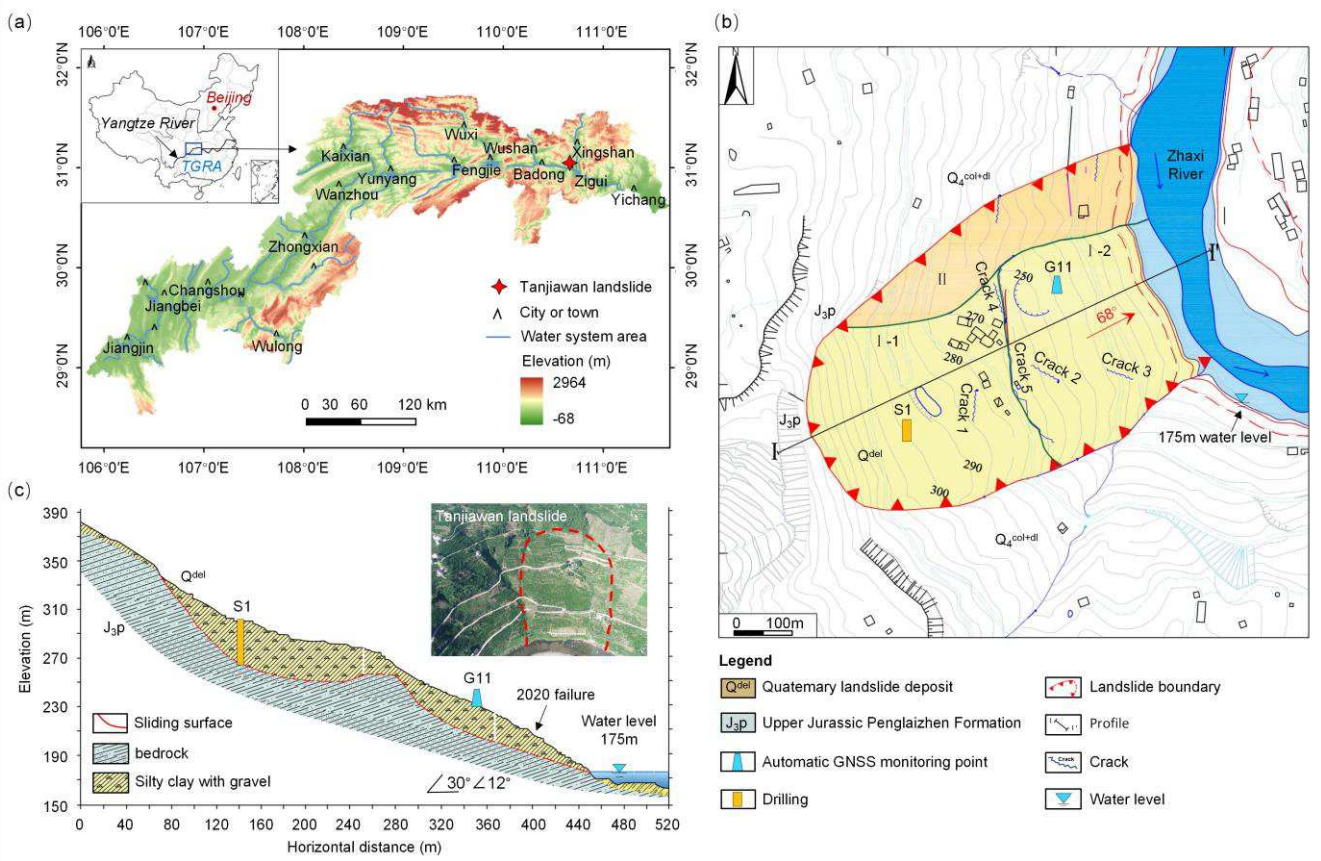


Fig. 2 illustrates the geographical location and monitoring point arrangement of the Tanjiawan landslide within the TGRA of China. Panel (a) presents the geographical location of the landslide, while panels (b) and (c) depict the plan view and cross-section of the landslide, respectively.

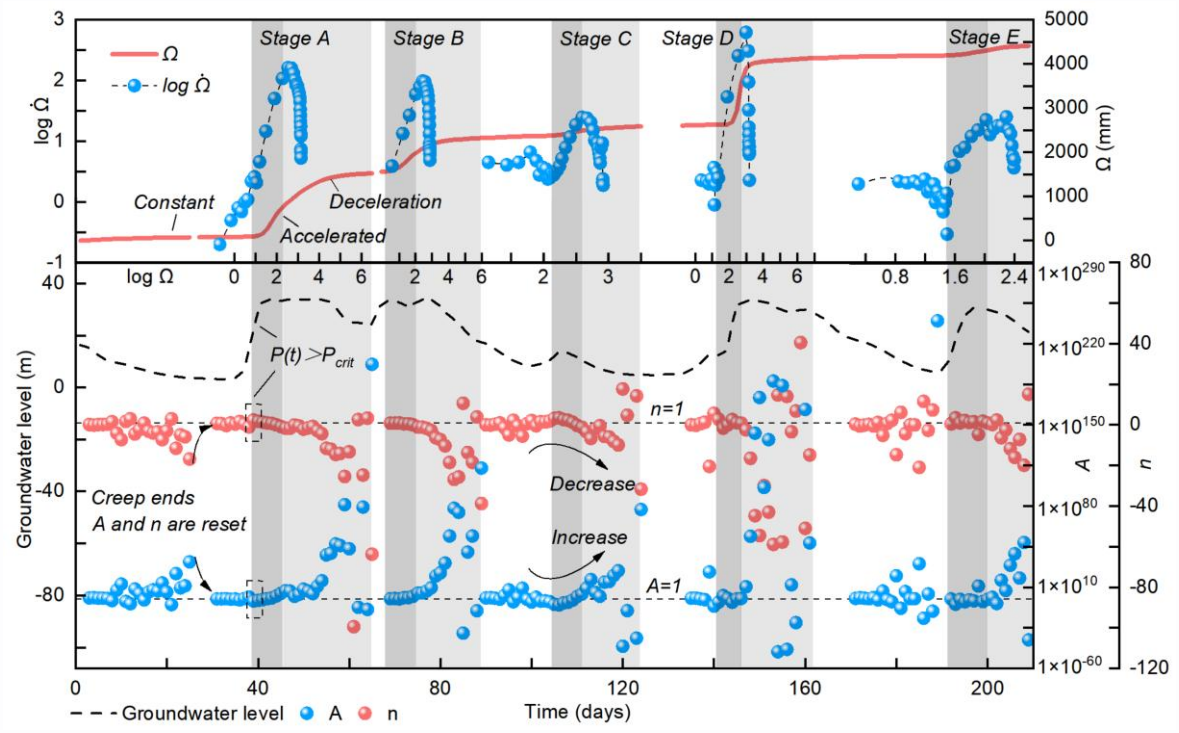


Fig. 3 illustrates the relationship between rate and displacement, highlighting the dynamic response characteristics of parameters A and n during five creep processes (from May to December 2020) of the

Tanjiawan landslide in the TGRA. The upper plot presents the displacement curves alongside the $log\dot{\Omega}-log\Omega$ relationship, Ω=surface movement (mm). The lower plot depicts the temporal variations of parameters A, n, and groundwater levels. The red line represents the displacement curve of the landslide, where a continuous increase in displacement indicates intensified endogenous damage. The shaded area illustrates that rising groundwater levels lead to an increase in the n value, suggesting that exogenous loads, particularly fluid pressure, contribute to the accelerated deformation of the landslide. This deformation is driven by the combined effects of both endogenous and exogenous factors.

The variation of model parameters reflects the relationship between the endogenous damage of materials and exogenous loads. A(t) characterizes the internal damage degree of materials: as A(t) approaches 0, the material exhibits enhanced mechanical strength and structural stability; an increase in A(t) signifies the continuous accumulation of endogenous damage. Upon the removal of external loads, the decrease and reset of A(t) correspond physically to the damage healing and recovery process of geological materials. n(t) represents the material's responsiveness to external factors: a decrease in n(t) indicates a rapid consumption of the material's displacement potential. When the rising groundwater level causes pore water pressure to exceed the critical threshold ($P(t) > P_{crit}$) (Fig. 3), the Tanjiawan landslide undergoes an abrupt state change, manifested by a sharp increase in n(t) and a rapid decrease in A(t). This characteristic aligns closely with the patterns observed in fault simulation experiments[13]: during the extreme pressurization process, where fluid pressure increased from 0.5 MPa to 5.4 MPa, deformation and pressure response first occurred at the injection point. Similarly, the Tanjiawan landslide exhibited significant deformation triggered when fluid pressure exceeded the critical threshold. Notably, the sharp increase in n(t) serves as a precursor signal indicating the transition from stable creep to accelerated shear failure. Meanwhile, the abrupt drop in A(t) during this phase characterizes accelerated creep rather than improved material stability. This phenomenon resembles the pattern where a sudden drop in stress and displacement triggers catastrophic landslides[26-27].

Under well-drained hydraulic conditions, rockslides may progress slowly over many years[28]. These landslides exhibit distinct characteristics compared to the intermittent failure patterns observed in the Tanjiawan landslide. Variations in pore fluid pressure can significantly alter the stress state within the landslide, resulting in sudden or delayed acceleration pulses, prolonged stable displacement rates, or runaway ruptures that culminate in catastrophic collapse[29]. A comparison of field data from the Tanjiawan landslide with laboratory pore pressure-step creep shear zone evolution experiments[15] indicates that increased water pressure can induce accelerated creep in landslides, with the

acceleration stage consistently accompanied by shear zone expansion and intensified geological damage. However, notable differences are evident: in laboratory experiments, shear zone compaction occurs immediately following the accelerated creep stage, manifesting as a typical undrained response where acceleration is associated with dilation, while deceleration triggers compaction. In contrast, after the accelerated creep of the Tanjiawan landslide, the deceleration stage may not involve immediate compaction. During this phase, although the creep rate diminishes due to the decay of exogenous load and a decrease in n(t), displacement continues to accumulate, leading to a persistent increase in the damage parameter A(t) while the shear zone maintains a dilation trend. Compaction of the shear zone occurs only as the creep process nears termination, at which point both A(t) and n(t) complete their reset and recovery (Fig. 3). Furthermore, the deceleration following accelerated creep is primarily attributed to the lack of stronger external dynamic driving forces. This stage reflects a reduced creep rate rather than an immediate onset of endogenous damage recovery in geological materials.

Discussion

Geological Hazard Cascading Effects in the Earth System

Geohazards within the Earth system do not occur in isolation; rather, they exhibit complex interconnections that can drive the generation of cascading effects (Fig. 4a). Earthquakes can directly trigger surface hazards such as landslides, while landslide-formed dammed lakes and reservoir impoundment processes may alter the crustal stress field, thereby inducing seismic activity[1]. Approximately 90% of earthquakes occur in regions with elevated Coulomb stress, resulting from the combined effects of direct loading and fluid diffusion. Indeed, terrestrial hazards such as earthquakes, wildfires, and floods evolve in cascading patterns[7]. Solid Earth processes, including earthquakes and volcanic eruptions, can trigger coseismic landslides; wildfires diminish soil erosion resistance and increase debris flow risks; and atmospheric processes, such as extreme precipitation and climate warming, exacerbate hazard susceptibility by altering hydrogeological conditions. These cascading processes may manifest immediately or be delayed for months to decades, with their dynamic characteristics regulated by multiple factors, including topography, geological material properties, and coupled hydro-biological interactions in the critical zone[9]. Clarifying the intensity, frequency, and mechanisms of multi-system interactions in cascading geological hazards is crucial for improving

multi-hazard risk assessment and enhancing societal disaster resilience, particularly in the context of rapid climate change and urban expansion in high-risk areas.

Previous studies have predominantly focused on the triggering effects of earthquakes on large-scale geological movements. However, processes such as Earth tides[30], reservoir impoundment[31] , hydraulic fracturing[32], and lake filling[33] can also induce earthquakes[34] by altering crustal stress through surface loading or fluid diffusion when the stress around active faults exceeds critical thresholds. Research has demonstrated that the heterogeneity of geological materials—such as crack distribution, pore spacing, stress fields, and fault roughness—exerts a decisive influence on the failure acceleration phase preceding catastrophic rupture[35-37]. For instance, fluid injection can reactivate faults and enhance fluid transport capacity in low-permeability faults, which has significant implications for geological carbon sequestration and subsurface energy storage[13], while also triggering earthquakes in natural earthquake swarms[38] and human-engineered energy extraction activities[39]. Increased pore pressure can directly drive seismic fault slip[40], while hydraulic fault properties mediate the feedback between permeability/porosity evolution and fault slip, thereby regulating the dynamic changes in pore pressure[14].

Analytical framework of endogenous-exogenous (A-n) coupling effects

The unified creep model we proposed, represented as $\dot{\Omega}(t)=A(t)\Omega^{n(t)}$, provides a comprehensive description of the entire process from creep to failure through the dynamic evolution of endogenous damage A and exogenous load n (Fig. 4b). In the decelerating creep stage, early displacement accumulation induces significant endogenous damage, resulting in high values of A, while the effects of exogenous load remain weak and continuously attenuate ($n < 0$). Although the high endogenous damage (A) can partially compensate for the weakening of exogenous loads, their coupled interaction maintains the geological mass in a low-speed creep state (Fig. 4c-d). In the steady-state creep stage, the evolution of endogenous damage stabilizes ($A\rightarrow1$), while exogenous disturbances persist at low intensity ($n\rightarrow0$). Both A and n exhibit low-amplitude fluctuations, with their coupled interaction determining the stability of the creep rate in the geological mass. During the accelerated creep stage, the impact of exogenous loading significantly intensifies ($n > 1$), while the accumulated endogenous damage from prior creep exacerbates, driving a continuous increase in the value of A. In stark contrast to the steady-state stage, this stage displays a synergistic leap characteristic between A and n, with their coupling effect triggering a catastrophic acceleration in the creep rate of the geological body. In

the post-failure stabilization stage, after material failure, the system gradually stabilizes with a simultaneous reset of A and n; the geological body then enters a dormant state, awaiting either the triggering of exogenous load or the accumulation of endogenous damage to a critical threshold that initiates a new creep cycle.

During the disaster cascade process, exogenous triggering events such as earthquakes, extreme precipitation, and volcanic activity lead to a significant increase in the n value, thereby inducing primary hazards such as landslides and debris flows. Concurrently, endogenous factors, including hillslope material degradation and hydro-geological coupling in the critical zone, regulate the sensitivity of geological bodies to subsequent disturbances through the dynamic evolution of the A value. The creep of geological bodies is influenced by both endogenous stability and exogenous loading: geological bodies with high endogenous stability (e.g., dense structure, high friction) can withstand substantial exogenous loads, whereas those with low endogenous stability (e.g., loose structure, low friction) are susceptible to failure under minor exogenous disturbances. The combination of endogenous stability degradation and intense exogenous loading can easily trigger sudden disasters, such as extreme rainfall-induced group-occurring landslides or earthquake-triggered instantaneous failures. For geological bodies demonstrating high endogenous stability, extreme exogenous loading or prolonged accumulation of endogenous damage is necessary to induce fracturing.

This model elucidates the disaster mechanism through the endogenous-exogenous A-n coupling approach and identifies the dominant factors at each creep stage. The decelerating creep stage is primarily governed by the accumulation of endogenous damage, characterized by an increase in parameter A and a decrease in parameter n. The steady-state creep stage is influenced by the coupling effect of both endogenous and exogenous factors, wherein parameters A and n exhibit small, stable variations. In contrast, the accelerated failure stage is predominantly driven by the simultaneous increase of both endogenous and exogenous factors, leading to an increase in parameters A and n. Thus, a complementary compensation effect exists between A and n. An increase in a single parameter does not necessarily lead to geological failure; rather, the synergistic increase of both parameters serves as the fundamental condition for the occurrence of catastrophic disasters.

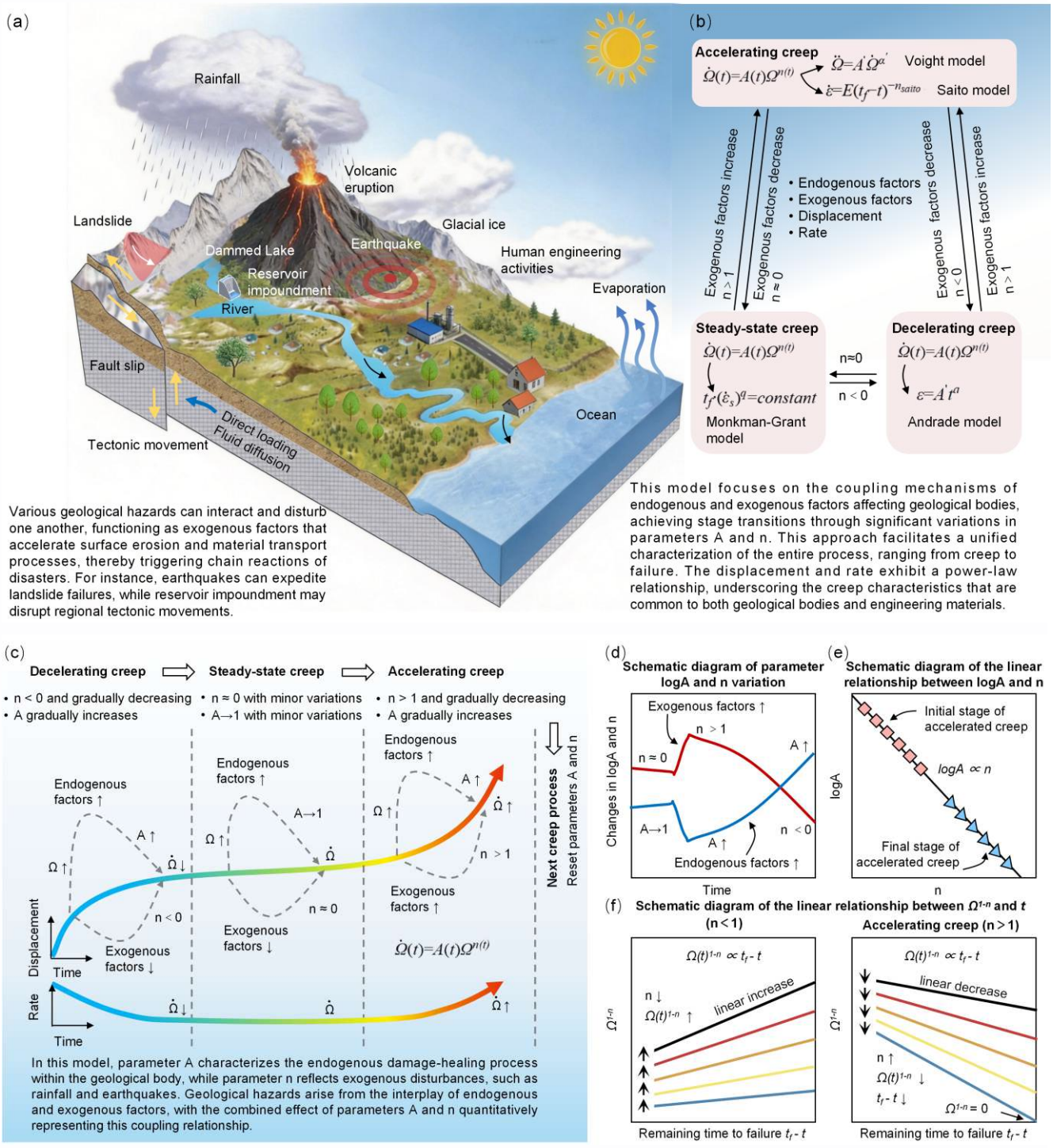


Fig. 4 illustrates the endogenous-exogenous coupling mechanism and geological hazard cascading effects. (a) It depicts the cascading effects of geological hazards within the Earth System, emphasizing that various geological hazards, including landslides, volcanic eruptions, glacial movements, and fault slips, are influenced by endogenous-exogenous coupling. (b) The model indicates that the relationship between displacement and rate follows a power law. Transitioning between creep stages is facilitated by variations in the parameter n, which allows for a unified characterization of the entire process from creep to failure. (c) The analytical framework of endogenous-exogenous (A-n) coupling effects is presented, where A and n quantify their coupling relationship and identify the dominant factors at each stage. (d) A schematic diagram illustrates the variations of logA versus n. (e) It also demonstrates the

linear relationship between logA and n. (f) Furthermore, a linear relationship between $\Omega^{(1-n)}$ and time t_f-t is established, which is utilized for predicting failure time.

Damage-healing-relocking process of fault zones under earthquake disturbances

The 2008 Wenchuan earthquake (Mw 7.9), recognized as a significant exogenous triggering event[4], caused substantial degradation of rock masses along the Longmenshan fault zone. The average velocity of the upper crustal Pg waves experienced an abrupt decline of approximately 4%, indicating intensified rock damage, which subsequently resulted in an increase in parameter A. Concurrently, the co-seismic slip rate of the fault sharply decreased, leading the fault zone into a decelerating creep phase characterized by diminished exogenous loading effects (a reduction in n). Although the rate of displacement accumulation slowed during this deceleration phase, it continued to progress, causing the damage parameter A to rise progressively. This increase in A could partially offset the reduction in exogenous loading (n), with the coupling effect between these two factors maintaining the geological body in a state of low-velocity creep. In the subsequent post-earthquake recovery stage, the Beichuan asperity was the first to reach a steady-state creep stage, with its rate continuously recovering. During this stage, the evolution of endogenous damage gradually stabilized (A→1), while exogenous disturbances remained at low levels (n→0), with the coupling effect governing the stability of the creep rate. In contrast, the Wenchuan asperity exhibited delayed recovery, with the A value remaining elevated and $n < 0$, which kept it in a decelerating creep stage. Following the 2013 Lushan earthquake (Mw 6.6), the regional tectonic loading and stress redistribution it triggered caused a sharp increase in the n value. Although the coseismic rate drop from the earthquake itself was brief, it significantly initiated accelerated healing of the Wenchuan asperity, leading to a temporary acceleration of local slip. At this juncture, A and n exhibited a characteristic of synergistic leap. Following the accelerated healing process, the fault enters a relocking stage characterized by enhanced endogenous stability, during which the parameters A and n are reset to low levels. For faults with high endogenous stability, new rupture phenomena, such as fault movement, are likely to occur only under extreme exogenous loads or through the long-term accumulation of endogenous damage.

Creep of granular materials under no obvious exogenous disturbance

Interestingly, previous experiments have reported sustained creep phenomena in granular materials, such as sand piles, even in the absence of significant exogenous disturbances[42-43]. In these cases, the degradation of particle roughness and frictional properties leads to an increase in the A

value. Even when the n value remains low, their synergistic effect can still induce deformation. Similarly, in scenarios of high material stability, characterized by an extremely low A value, strong external disturbances with a high n value may initiate creep failure processes, as these disturbances continuously amplify internal material damage. This observation elucidates the intrinsic mechanisms behind various geological hazards that occur in mountain masses following prolonged geological evolution and tectonic activities. Furthermore, although metal alloys exhibit high strength, they are not immune to creep phenomena under conditions of high temperature, high stress, and prolonged duration testing[23].

Slow sliding of giant rock landslides

Giant rock landslides exhibit high sensitivity to hydrological forces and may undergo catastrophic failure after centuries of slow creep due to climate warming. However, the transition mechanism from gradual sliding to collapse remains unclear[15]. Natural slopes in subcritical stress states respond to exogenic geomorphic perturbations, such as river incision and glacial/deglacial processes, which drive an increase in the exogenous parameter n value and trigger progressive rock fracturing[44]. This long-term fracturing process promotes the continuous growth of the endogenous damage parameter A-value, accompanied by an enhancement in permeability, until strain localization occurs in the basal shear zone[45]. As strain accumulates in the shear zone, the fine-grained gouge thickens and becomes more abundant, reducing permeability and facilitating the development of a perched aquifer system[46]. Meanwhile, damage accumulation in the basal shear zone maintains the A value at elevated levels, thereby sustaining slope creep. As the shear zone matures, creep becomes increasingly dominated by hydro-mechanical coupling. Additionally, landslide creep is modulated by endogenous stabilizing forces conferred by the geological context. Special geological units with larger contact areas—such as landslide necks, irregular hoppers, and the interfaces between landslide necks and pull-apart basins—can provide additional endogenous stabilizing forces by increasing contact area, thereby suppressing further A value growth and n value fluctuations to inhibit deformation[9].

Volcanic flank collapse and glacier surge

Volcanic islands are particularly vulnerable to flank collapses due to their fragile basement and fractured media, which can trigger secondary disasters such as landslides and pyroclastic flows entering the sea, resulting in a cascading chain of compound hazards. Prior to the collapse of the Anak

Krakatau volcano sector, prolonged magmatic activity and hydrothermal processes weakened the volcanic media and compromised its structural integrity, leading to a continuous increase in the endogenous damage parameter A value. This established the internal foundation for the initiation of creep. Exogenous triggering events, such as eruptive pulses and seismic disturbances, subsequently elevated the n value. The synergy of these factors facilitated the transition of the volcanic flank from steady-state creep to accelerated creep, ultimately culminating in collapse[17]. Glacier surges are induced by changes in basal shear stress or resistance at the ice-bed interface, regulated by endogenous factors such as glacier geometry and subglacial media, while climatic factors (temperature and precipitation) act as significant exogenous triggers. Taking Kongsvegen Glacier in the Svalbard archipelago as an example, enhanced surface ablation allows meltwater to reach the glacier bed, resulting in a substantial increase in the n value. The elevated basal water pressure reduces bed friction, prompting rapid glacier sliding and the formation of surface crevasses[47-50]. The aforementioned processes confirm that rate variation serves as a sensitive indicator of the medium's state and stress evolution, which aligns with the unified creep model's description of the entire creep-to-failure process, expressed as $\dot{\Omega}(t)=A(t)\Omega^{n(t)}$.

Applications

LogA exhibits a linear relationship with the variable n (Fig. 4e), simplifying the unknown parameters to a single variable, n. This relationship provides a theoretical basis for predicting later-stage evolution using early monitoring data. More critically, $\Omega^{(1-n)}$ demonstrates a clear linear pattern with the remaining time to failure, $t_f - t$: when $n > 1$, they exhibit an inverse relationship. Based on this observation, by linearly extrapolating the $\Omega^{(1-n)}$-t curve to $\Omega^{(1-n)} = 0$, the time of failure can be estimated (Fig. 4f). This model eliminates the need for direct measurement of difficult-to-obtain stress fields, requiring only directly observable displacement data from GNSS or InSAR to complete predictions, thereby enhancing engineering practicality.

This study demonstrates the predictive capability of the model through case studies on accelerated creep prior to landslide failure, accelerated creep before glacier rupture, and multi-stage creep in alloys. It emphasizes real prediction scenarios based on extrapolation from early-stage data. The original time-series data can be smoothed to obtain more robust time series[21,51]. Furthermore, when performing linear regression on the feature sequence $\Omega^{(1-n)}$, the coefficient of determination (R^2)

must exceed 0.9 to ensure the reliability of the extrapolated prediction of failure time t_f. If R^2 falls below 0.9, it is advisable to discard older data to minimize subjectivity in defining the initial point.

The first case under examination is the Vaiont landslide in Italy[20]. On October 9, 1963, a landslide measuring approximately 2 kilometers in width was initiated on the Monte Toc slope in the Dolomite region of the Italian Alps, located about 100 kilometers north of Venice, at an elevation ranging from 1100 to 1200 meters. This elevation is 500 to 600 meters above the valley floor. The event concluded 70 days later with the rapid movement of approximately 0.3 cubic kilometers of rock sliding into a dam reservoir at a velocity of 20 meters per second. The high speed of the slide triggered a water surge within the reservoir, resulting in the overtopping of the dam and the tragic loss of 2500 lives in the downstream villages of Longarone, Pirago, Villanova, Rivalta, and Fae.

The time-varying functions $A(t)$ and $n(t)$ are derived through real-time fitting of adjacent time points in the $log\dot{\Omega}$–$log\Omega$ plot. These values are subsequently substituted into Equation (4a) to forecast displacement. When $t_f - t$ = 20 days (n = 1.27, A = 0.058), the prediction curve effectively captured the acceleration trend of the Vaiont landslide (Fig. 8). As exogenous factors increased, leading to an increase in n to 2.23 ($t_f - t$ = 4 days), the predicted displacement gradually aligned with the actual displacement curve, thereby enhancing prediction accuracy (MAPE = 4.9%). In addition to predicting displacement, it is also possible to forecast the remaining failure time of the landslide. Both the $\Omega^{(1-n)}$ extrapolation method employed in this model and the Voight inverse rate method intersect with the criterion line at $t_f - t$ = 4 days, effectively predicting landslide failure (Fig. 5a). Notably, in the $\Omega^{(1-n)}$ extrapolation method, a larger n is associated with a smaller $t_f - t$ By continuously monitoring $A(t)$ and $n(t)$ in real time, the prediction results can be dynamically updated, enhancing accuracy as the failure event approaches.

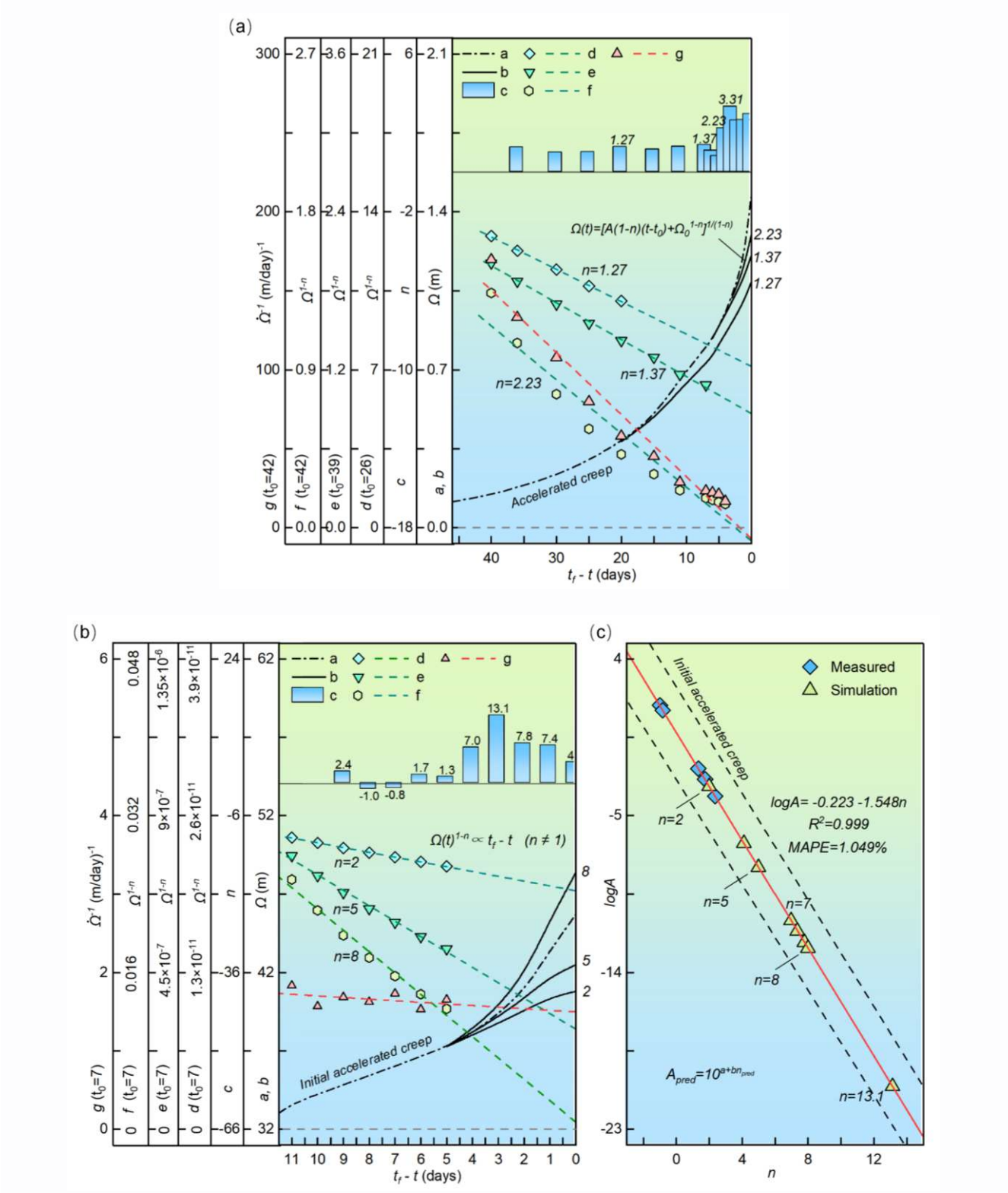


Fig. 5 illustrates the prediction results for creep and failure time in geological materials. Subfigure (a) presents the predictions of displacement and failure time for the Vaiont landslide in Italy. Curve (a) represents the actual displacement, while curve (b) depicts the predicted displacement based on equation (4a) (with $n > 1$). Curve (c) shows the daily variation of n, and curves (d), (e), and (f) display the fitting of $\Omega^{(1-n)}$ (for $n > 1$) data along with the prediction of the remaining failure time t_f - t. Subfigure (g) further demonstrates the prediction of t_f - t using the inverse rate method. Subfigure (b)

illustrates the displacement and failure time prediction preceding the rupture of the glacier at Grandes Jorasses, Italy. Finally, subfigure (c) indicates that by analyzing the linear relationship between $logA$ and n during the accelerated creep stage, the two parameters A and n can be simplified into a single parameter. Consequently, only the value of n is necessary to predict displacement and failure time.

The second case study focuses on the Glacier at Grandes Jorasses, Italy[6], specifically a hanging cold glacier located on the southern face at an elevation of 3,950 meters above sea level. Surface displacements of this glacier were measured using a robotic total station equipped with multiple reflectors, achieving an accuracy of approximately 1 centimeter. A significant volume of approximately 105,000 cubic meters of ice calved during two consecutive events on September 23 and 29, 2014. Our analysis emphasizes the first calving event. It is well-documented that glaciers exhibit smooth, accelerating creep characteristics for several months prior to rupture. Therefore, we concentrate on the initial rupture event to assess the model's capacity to predict the transition from the high-damage stage to the low-damage stage in advance.

By performing real-time fitting on the $log\dot{\Omega}-log\Omega$ plot of two adjacent time-sequence points, the time-varying parameters $A(t)$ and $n(t)$ were obtained. Linear fitting using Equation (9a) yielded initial acceleration stage parameters of a = -0.223 and b = -1.548 (R^2 = 0.999). Setting n_{pred} to range from 2 to 8, A_{pred} was calculated with Equation (9b). The (A_{pred}, n_{pred}) values were subsequently substituted into Equation (4a) to predict the displacement during the acceleration stage (Fig. 5b-c). When n_{pred} was set to 8, the predicted curve closely aligned with the actual acceleration trend, effectively capturing the evolutionary characteristics of ice acceleration and fracture. Furthermore, the prediction error between A_{pred} and the actual A resulted in a Mean Absolute Percentage Error (MAPE) of 1.049%, thereby validating the stability of the $logA$-n linear relationship and the reliability of the advance prediction.

The inverse rate method is significantly dependent on data obtained during the late acceleration stage, complicating the effective prediction of failure time based on early observations (Fig. 5b). In this model, when n_{pred} = 8, the $\Omega^{(1-n)}$ extrapolation method facilitates an early prediction at t_f - t = 5 days. In contrast, the actual glacier exhibits n_{max} = 13.1, allowing an early warning to be activated upon detecting n_{crit} = 8. This model enables experienced observers to identify the failure threshold n_{crit} of the failure window at an earlier stage. Essentially, the inverse rate (Ω^{-1}) method is a static model characterized by strictly constrained parameters and relationships, which limits its ability to adapt to the complex creep behaviors observed in real-world scenarios[52-53]. In contrast, our method ($\Omega^{(1-n)}$)

incorporates a time-varying exogenous factor, n, which facilitates the identification of the creep stage of materials, thus providing enhanced flexibility in predicting the time to failure.

The third case involves the multi-stage creep prediction of alloys. Similar to the first case, the real-time fitting-dynamic prediction method is employed. The time-varying parameters $A(t)$ and $n(t)$ are obtained through $log\dot{\Omega}-log\Omega$ fitting, which are subsequently substituted into Equation (4a) to predict the creep strain. For the UNS N10003 alloy[23], under constant stresses of 250 MPa, 275 MPa, 320 MPa, and 380 MPa at 650° C, the creep behavior transitions from a constant rate to an initial acceleration stage (at approximately t = 140 h, A = 0.5, n = 0.26; at approximately t = 280 h, A = 0.16, n = 1). The predicted curves closely match the actual strains (Fig. 6). For Ti-6Al and Ti-6242 alloys, creep occurs under loads of 716 MPa and 931 MPa, respectively[4], with data corresponding to the deceleration creep stage (A = 0.002, n = -5.2 at approximately t = 20,000 seconds), where the creep rate continues to decrease, and the predicted curve accurately captures the characteristics of this decreasing rate.

The differences in creep behavior among these alloys can be attributed to the specific testing conditions employed: UNS N10003 was subjected to high temperature, high stress, and prolonged duration, whereas Ti-6Al and Ti-6242 were evaluated under low temperature, high stress, and short duration. These conditions represent two typical scenarios of large strain acceleration and small strain deceleration. It is evident that the evolution of $A(t)$ and $n(t)$ is influenced by the testing conditions, which directly determine the creep behavior.

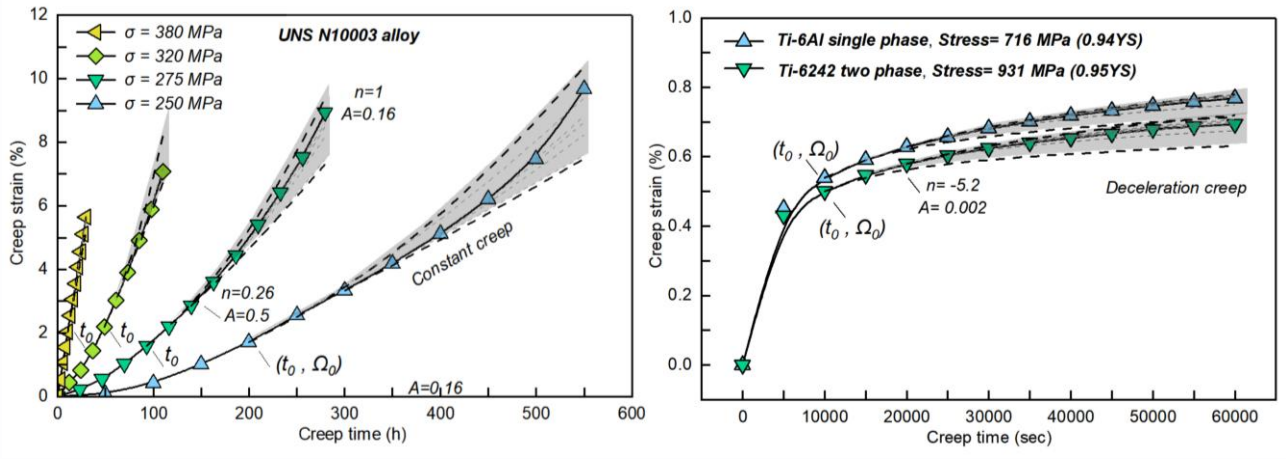


Fig. 6 presents the prediction results of multi-stage creep in alloys. The solid lines illustrate the actual strain, while the dashed lines denote the predicted strain. On the left, the predicted strain ε (%) versus time t (h) curves for the UNS N10003 alloy at 650°C are depicted under varying pressures of 250 MPa, 275 MPa, 320 MPa, and 380 MPa. Conversely, on the right, the predicted strain ε (%) versus

time t (sec) curves for the Ti-6Al and Ti-6242 alloys are displayed under pressures of 716 MPa and 931 MPa, respectively.

Methods

Displacement and rate prediction methods

This model describes the unified creep behavior of materials during the deceleration, constant, and acceleration stages of creep. The coupled equations for rate, displacement, and time are derived in the subsequent sections. When $A(t)$ and $n(t)$ are treated as constants, Equation (1) simplifies to an ordinary differential equation. By employing the method of separation of variables and performing subsequent integration, we obtain the following results:

For n=1:

$$\Omega(t)=\Omega_0 e^{A(t-t_0)} \tag{3a}$$

$$\dot{\Omega}(t)=A\Omega_0 e^{A(t-t_0)} \tag{3b}$$

or for $n\neq 1$:

$$\Omega(t)=\left[A(1-n)(t-t_0)+\Omega_0^{1-n}\right]^{\frac{1}{1-n}} \tag{4a}$$

$$\dot{\Omega}(t)=A\left[A(1-n)(t-t_0)+\Omega_0^{1-n}\right]^{\frac{n}{1-n}} \tag{4b}$$

This analytical solution describes the creep behavior across material lifetimes: when $n > 1$, both Ω and $\dot{\Omega}$ accelerate until failure occurs within a finite time; when $0 < n < 1$, the rate increases slowly and stabilizes; and when $n < 0$, the rate decays, corresponding to the deceleration stage.

Taking the Tanjiawan landslide Stage A (June 13 - July 17, 2020) as a case study, the range of ($logA$, n) values was linearly fitted in the $log\dot{\Omega}-log\Omega$ plot. Multiple sets of (A, n) were utilized to predict the displacement and rate curves, as illustrated in Fig. 7.

The results indicate that during the constant, acceleration, and two deceleration creep stages, endogenous factor A initially decreased before increasing, with values of 0.66, 0.38, 1.9×10^{5}, and 1.2×10^{48}, respectively. In contrast, exogenous factor n initially increased before decreasing, with values of approximately 0.62, 1.12, -1.15, and -14.96, respectively. The coefficient of determination (R^2) was greater than 0.97 for displacement and greater than 0.8 for rate. This verifies that the coupling of endogenous and exogenous factors A and n can effectively describe and predict full-life-cycle creep.

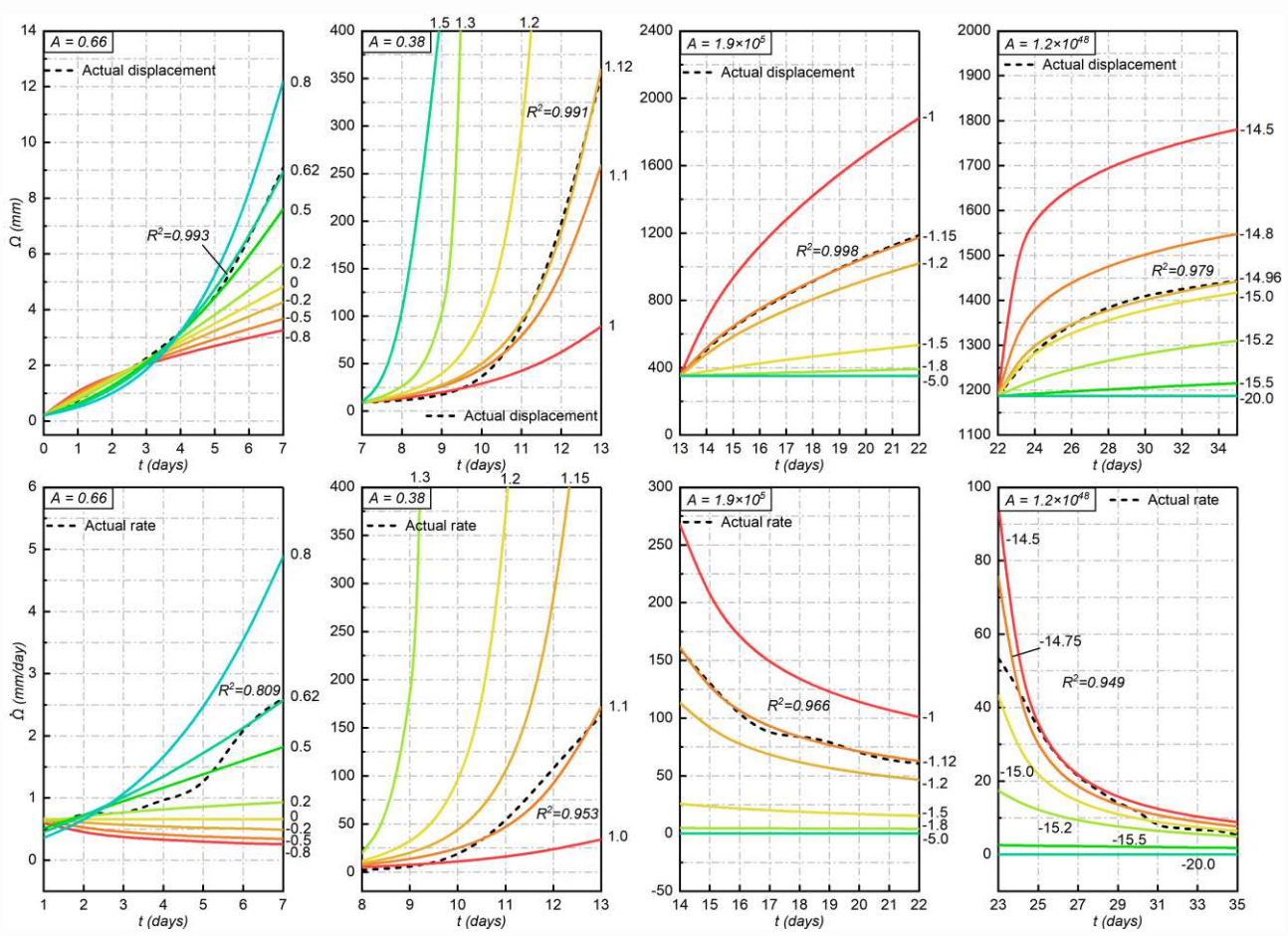


Fig. 7 illustrates the analytical solution predictions for creep during Stage A of the Tanjiawan landslide. The upper section presents the displacement (Ω) versus time (t) curves, which include predictions based on multiple parameters. In contrast, the lower section depicts the rate ($\dot{\Omega}$) versus time (t) curves, also derived from various parameter predictions. The initial conditions are defined as $t_0 = 0$ and $\Omega_0 = 0.2$ mm. Predictions were generated using equations (3a) and (3b) for the case when $n = 1$, while equations (4a) and (4b) were applied for $n \neq 1$.

Failure time prediction method

Prediction of creep rupture time. When $n>1$, at $t = t_f$, $\Omega \to \infty$, obtained from equation (4b):

$$A(1-n)(t_f-t_0)+\Omega_0^{1-n}=0$$

Substituting the above equation into equation (4b), the accelerated creep rate expression is obtained:

$$\dot{\Omega}(t)=A\left[A(n-1)(t_f-t)\right]^{\frac{n}{1-n}} \tag{5a}$$

Here, the exponent $\frac{n}{1-n}<0$, indicating that the rate increases as the remaining time to failure t_f-t decreases. The inverse rate expression is:

$$\dot{\Omega}(t)^{-1}=A^{-1}\left[A(n-1)(t_f-t)\right]^{\frac{n}{n-1}} \tag{5b}$$

The exponent $\frac{n}{1-n} > 0$ indicates that the inverse rate decreases to zero as the remaining time to failure $t_f - t$ diminishes.

Based on the fundamental relation $\ddot{\Omega} = A' \Omega^{\alpha'}$, Voight provided a similar inverse rate expression[2]:.

$$\dot{\Omega}(t)^{-1} = \left[A'(1-\alpha')(t-t_0) + \dot{\Omega}_0^{1-\alpha'} \right]^{\frac{1}{\alpha'-1}} \tag{6}$$

Equations (5b) and (6) embody the same physical principle, both illustrating a power-law relationship between the inverse rate and time. This relationship serves as the theoretical foundation for the inverse rate prediction method.

Assuming that $\Omega \to \infty$, which occurs only when $n > 1$, the term within the brackets of equation (4a) will asymptotically approach zero as time t progresses. Consequently, the failure time can be determined as follows:

$$t_f - t_0 = \frac{\Omega_0^{1-n}}{A(n-1)}$$

By introducing Ω at the current time t, we obtain:

$$t_f - t = \frac{\Omega^{1-n}}{A(n-1)} \tag{7}$$

Equation (7) indicates that the remaining time to failure $t_f - t$ is proportional to the current Ω^{1-n}.

For n≠1, equation (4a) can be rewritten as a standard linear equation:

$$\Omega(t)^{1-n} = [A(1-n)] \cdot t + \left[\Omega_0^{1-n} - A(1-n)t_0 \right] \tag{8a}$$

For $t_0 = 0$,

$$\Omega(t)^{1-n} = A(1-n) \cdot t + \Omega_0^{1-n} \tag{8b}$$

In the equation, the slope is given by $A(1-n)$, while the intercept is a constant represented by $\Omega_0^{1-n} - A(1-n)t_0$. This serves as the theoretical foundation for the linear relationship between $\Omega(t)^{1-n}$ and time t. When $n < 1$, $\Omega(t)^{1-n}$ is directly proportional to time t; when $n > 1$, $\Omega(t)^{1-n}$ is inversely proportional to time t, and as t increases, $\Omega(t)^{1-n}$ gradually decreases.

To achieve early warning, we developed a method for predicting creep and failure times during high-damage stages based on observations from low-damage stages, guided by the following three axioms. Axiom 1: Invariance of linear constraints in parameter space. During individual creep events,

the logarithm of the parameter *log A* shows a linear relationship with the parameter n, as indicated by an R^2 value approaching 1, as illustrated in Fig. 8a-c. Axiom 2: Physical inevitability of accelerated failure. Once materials enter the acceleration stage, damage becomes irreversible under sustained loading, leading to deformation that ultimately results in failure. Axiom 3: Deductibility of stage parameters. The predicted values of A_{pred} and n_{pred} for future stages can be estimated based on historical data or experiences with similar materials, thus narrowing predictions from an infinite array of possibilities to a finite set of reasonable scenarios.

$$logA=a+b\cdot n \tag{9a}$$

$$A_{pred}=10^{a+b\cdot n_{pred}} \tag{9b}$$

In this equation, the parameters (a, b) are defined by the early-stage creep displacement and rate. This suggests that the material's ultimate creep behavior is dictated by these early-stage parameters (a, b), allowing for the prediction of the evolution of the high-damage stage based on data from the low-damage stage.

Low-damage stage parameter fitting involves obtaining multiple sets of instantaneous parameters ($logA$, n) through the $log\dot{\Omega}–log\Omega$ plot, followed by determining the parameters (a, b) by fitting them with Equation (9a). For high-damage stage parameter prediction, we propose the parameter n_{pred} and calculate A_{pred} using Equation (9b). In the full-stage evolution prediction, we substitute (A_{pred}, n_{pred}) into the analytical solutions for displacement and rate, along with the time-to-failure formula, to predict creep behavior and remaining lifespan.

Taking the Tanjiawan landslide Stage D (September 25-October 6, 2020) as a verification example (Fig. 8d-f), this stage transitioned from steady creep to accelerated creep, which aligns with the predicted scenario of a transition from low to high damage. Based on data from the steady creep stage, values of a = 0.31 and b = -1.12 were obtained. By setting n_{pred} = 2, the predicted displacement curve demonstrated a high degree of consistency with the actual acceleration stage. Utilizing the $\Omega(t)^{1-n}$ extrapolation method, when n_{pred} = 2, the predicted curve intersected with the criterion line ($\Omega(t)^{1-n}$=0.001 → 0) on the day of failure. In engineering practice, where $\Omega(t)^{1-n} \neq 0$, it is necessary to extrapolate the $\Omega(t)^{1-n}$ curve until it intersects with the x-axis, or alternatively, to establish a criterion for the critical $\Omega(t)^{1-n}$ threshold.

Based on this, we can establish a bidirectional application system combining forward warning and reverse prediction. By setting the failure displacement $\Omega_f \approx 1000$ mm and inversely deriving through $\Omega(t)^{1-n} \rightarrow 0.001$, we obtain the critical threshold $n_{crit} = 2$. In engineering practice, when monitoring shows n exceeds this value, an early warning can be triggered. Conversely, if the critical failure value $n_{crit} = 2$ is known, the failure displacement $\Omega_f \approx 1000$ mm can be calculated inversely through $\Omega(t)^{1-n} \rightarrow 0.001$.

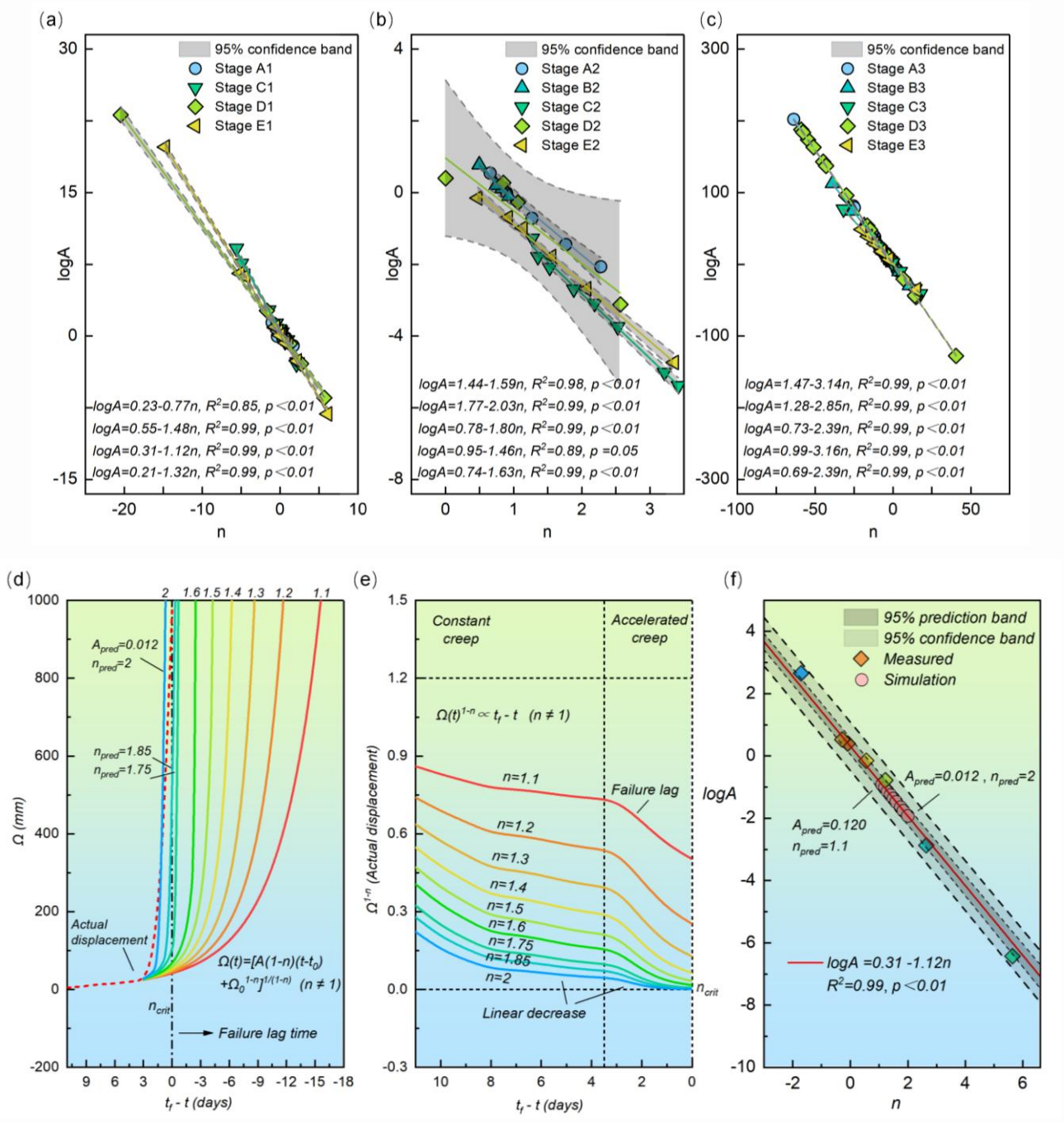


Fig. 8 a-c illustrate the linear relationship between *logA* and *n* during Stages A-E of the Tanjiawan landslide. d presents the predicted displacement (Ω) for Stage D, with an initial displacement (Ω_0) of

2.3 mm at time (t_0) equal to 0. e displays the calculated results of $\Omega(t)^{1-n}$ for Stage D. f demonstrates the linear fit of $logA$ against n for Stage D, from which the corresponding A value can be derived by substituting n.

Correlation between the Unified Creep Model and other models

The unified creep model proposed in this study, expressed as $\dot{\Omega}(t)=A(t)\Omega^{n(t)}$, features a dynamic power-law relationship between rate and displacement as its core mechanism. This model exhibits structural similarities with multiple creep models in the fields of materials science and geotechnical engineering. By defining time-varying parameters in a physical context, we establish a unified interpretative framework for various creep models.

The Voight model for predicting volcanic eruptions and landslides is expressed as follows[2,11]:

$$\ddot{\Omega}=A'\dot{\Omega}^{\alpha'} \tag{10}$$

In the equation, A' and α' are empirical constants. By differentiating the model $\dot{\Omega}=A\Omega^n$ and eliminating Ω, the Voigt expression can be derived:

$$\begin{cases} \ddot{\Omega}=A'\dot{\Omega}^{\alpha'} \\ A'=nA^{\frac{1}{n}} \\ \alpha'=2-\frac{1}{n} \end{cases} \tag{11}$$

In this model, A' and α' are defined as composite parameters derived from A and n. When $n > 1$, we conducted a statistical analysis of the instantaneous n values observed in materials such as landslides and volcanic eruptions, which range from 1 to 15.4 (Fig. 1). This analysis yielded α' values between 1 and 1.94, aligning with extensive experimental observations[54] that indicate α' approaches 2. Furthermore, the model effectively accommodates variable loading scenarios through the time-varying characteristics of $A(t)$ and $n(t)$, thereby eliminating the need to introduce stress ratio correction terms, such as $(\sigma/\sigma')^m$.

By eliminating the displacement Ω from Equation (7b), where $A'=nA^{\frac{1}{n}}$ and $\alpha'=2-\frac{1}{n}$, the model $\dot{\Omega}=A\Omega^n$ can be transformed into the predicted failure time expression of the Voigt model.

$$t_f-t=\frac{\dot{\Omega}^{1-\alpha'}}{A'(\alpha'-1)}$$

In the equation, when $n \to \infty$, $\alpha' \to 2$, $\dot{\Omega}^{1-\alpha'}$ approaches $\dot{\Omega}^{-1}$, indicating that the remaining time $t_f - t$ is linearly and positively correlated with $\dot{\Omega}^{-1}$. This is the inverse rate prediction method for failure time.

The Saito equation describes accelerated creep behavior in materials such as soil[3]. This equation can be expressed in the following form:

$$\dot{\varepsilon} = E(t_f - t)^{-n_{saito}} \tag{12}$$

In the equation, $\dot{\varepsilon}$ represents the creep rate, t_f denotes the time to failure, and E and n_{saito} are empirical constants. When $n > 1$, Equation (5a) can be reformulated into the Saito expression.

$$\begin{cases} \dot{\Omega} = E(t_f - t)^{-n_{saito}} \\ E = A^{\frac{1}{1-n}}(n-1)^{\frac{n}{1-n}} \\ n_{saito} = \frac{n}{n-1} \end{cases} \tag{13}$$

The Andrade model characterizes the initial creep behavior of various metals and alloys under conditions of low temperature, low stress, and small strains (less than 2×10^{-3}). The mathematical expression of the model is as follows[4]:

$$\varepsilon = A' t^a \tag{14}$$

In the equation, A' and a are constants, while the time exponent a characterizes the rate of creep depletion. A smaller value of a indicates a faster depletion rate in the creep process.

When $n < 0$, $t_0 = 0$, and $\Omega_0 \to 0$, the analytical solution in Equation (4a) simplifies to the Andrade expression form:

$$\begin{cases} \Omega = A' t^a \\ A' = [A(1-n)]^{\frac{1}{1-n}} \\ a = \frac{1}{1-n} \end{cases} \tag{15}$$

When the value of n is smaller, the displacement potential energy of the material depletes more rapidly, resulting in a smaller value of a. This observation aligns with the pattern described by the Andrade model. Specifically, when $n = -2$, $a = 1/3$, which corresponds precisely to the typical Andrade creep characteristic.

The Monkman-Grant expression is a classical model that describes the creep rupture behavior of materials. Its formulation is as follows[5]:

$$t_f (\dot{\varepsilon}_s)^q = constant \tag{16}$$

In the equation, t_f is the fracture time, $\dot{\varepsilon}_s$ is the steady-state creep rate, and q is the material constant. For $t_0 = 0$, equation (4a) transforms into $t_f = \frac{\Omega_f^{1-n} - \Omega_0^{1-n}}{A(1-n)}$, equation (1) transforms into $\dot{\Omega}_f^{\,q} = (A\Omega_0^{\,n})^q$, and by combining equation (4a) and equation (1), we obtain:

$$t_f \dot{\Omega}_f^{\,q} = \frac{\Omega_f^{1-n} - \Omega_0^{1-n}}{1-n} A^{q-1} \Omega_0^{nq}$$

For, as $n \to 0$, a similar form of the Monkman-Grant expression is obtained:

$$t_f \dot{\Omega}_f^{\,q} = (\Omega_f - \Omega_0) A^{q-1} = constant \tag{17}$$

When $q=1$, $t_f \dot{\Omega}_f = \Omega_f - \Omega_0$.

By unifying the classical creep theories of Voigt, Saito, Andrade and Monkman-Grant within a single framework, this study establishes a common theoretical foundation for predicting creep and failure across diverse material systems. The dynamic evolution laws of the parameters $A(t)$ and $n(t)$ provide new insights for a deeper understanding of these classical models, while also elucidating the intrinsic connections that exist between them.

The improvement directions of this model encompass two primary aspects: First, embedding this constitutive relation within continuum mechanics equations to establish a field-scale creep model, which facilitates spatial predictions of the entire creep process within geological bodies. Second, by employing an approach akin to Earth system models that integrate atmospheric, oceanic, and terrestrial processes, the model effectively couples the creep process with exogenous factors such as rainfall and earthquakes. This coupling enables the quantification of the influence of various exogenous processes through the construction of the function n(t).

Acknowledgements

We gratefully acknowledge the support received from the National Field Observation and Research Station of Landslides in the Three Gorges Reservoir Area of Yangtze River, China Three Gorges University, and the College of Civil Engineering & Architecture at China Three Gorges University. Additionally, this research was financially supported by the National Natural Science Foundation of China (Grants No. 42172303 and 42577221).

Declaration of Competing Interest

The authors declare that they have no known competing financial interests or personal relationships that could have appeared to influence the work reported in this paper.

Data availability

The data analyzed in this study originate from the project titled "Professional Monitoring and Early Warning of Geological Hazards in Zigui County, Three Gorges Reservoir Area," along with literature data indexed in the Web of Science. The data supporting the results of this study are available within the article and its supplementary information. All other relevant data can be obtained from the corresponding author(s) upon reasonable request.

References

(1)Zhang, Z., Liu, M., Tan, Y.J. et al. Landslide hazard cascades can trigger earthquakes. Nat Commun 15, 2878 (2024).

(2)Voight, B. 1988. A method for prediction of volcanic eruptions. Nature, 332, 125-130.

(3). Saito, M. Proc. 7th int. Conf. Soil Mech. Found Engng 2, 677-683 (1969).

(4)T. Neeraj, D.-H. Hou, G.S. Daehn, et al. 2000. Phenomenological and microstructural analysis of room temperature creep in titanium alloys. Acta Materialia, 48(6): 1225-1238.

(5). Monkman, F.C. & Grant, N.J. Proc. Am. Soc. Test. Mater. 56, 593-605 (1956).

(6)Lei, Q., Sornette, D. 2025. Unified failure model for landslides, rockbursts, glaciers, and volcanoes. Commun Earth Environ 6, 390.

(7)Brian J. Yanites et al., 2025. Cascading land surface hazards as a nexus in the Earth system. Science388, eadp9559.

(8)Palmer, J. 2017. Creeping earth could hold secret to deadly landslides. Nature 548, 384–386.

(9)Hu, X., Bürgmann, R., Schulz, W.H. et al. 2020. Four-dimensional surface motions of the Slumgullion landslide and quantification of hydrometeorological forcing. Nat Commun 11, 2792.

(10)Fukuzono, T. 1985. A new method for predicting the failure time of a slope. Proc. IVth Intern. Conf. and Field Workshop on Landslides, Tokyo, 145–150.

(11)Voight, B. 1989. A Relation to Describe Rate-Dependent Material Failure. Science, 243, 200-203.

(12). Lei, Qinghua , Sornette, Didier, 2025. Endo-exo framework for a unifying classification of episodic landslide movements: Implications for forecasting catastrophic failures.Sci. Adv.11,eady9141.

(13)Cappa, F., Guglielmi, Y., Nussbaum, C. et al. 2022. Fluid migration in low-permeability faults driven by decoupling of fault slip and opening. Nat. Geosci. 15, 747–751.

(14)Zhu, W. et al. 2020. Fault valving and pore pressure evolution in simulations of earthquake sequences and aseismic slip. Nat. Commun. 11, 4833.

(15)Agliardi, F., Scuderi, M.M., Fusi, N. et al. 2020. Slow-to-fast transition of giant creeping rockslides modulated by undrained loading in basal shear zones. Nat Commun 11, 1352.

(16)Iverson, R. M. 2005. Regulation of landslide motion by dilatancy and pore pressure feedback. J. Geophys. Res.: Earth Surf. 110, F02015.

(17)Walter, T.R., Haghshenas Haghighi, M., Schneider, F.M. et al. 2019. Complex hazard cascade culminating in the Anak Krakatau sector collapse. Nat Commun 10, 4339.
(18)Liu, Chengli et al., 2026. Simple unilateral rupture of the great Mw 8.8 2025 Kamchatka earthquake. Science391, 812-817.
(19)Ren, M., Dai, F., Han, L. et al. 2024. Displacement prediction for landslide with step-like behavior based on stacking ensemble learning strategy. Stoch Environ Res Risk Assess 38, 3895–3906.
(20)Helmstetter, A., D. Sornette, J.-R. Grasso. et al. 2004. Slider block friction model for landslides: Application to Vaiont and La Clapière landslides, J. Geophys. Res., 109, B02409.
(21)Lacroix, P., Huanca, J., Albinez, L., & Taipe, E. 2023. Precursory motion and time-of-failure prediction of the Achoma landslide, Peru, from high frequency PlanetScope satellites. Geophysical Research Letters, 50, e2023GL105413.
(22)Raimbault, B., Jolivet, R., Calais, E., Fukushima, Y., & Symithe, S. 2025. Weak and shallow secondary frictional faults revealed by large earthquakes in Haiti. Geophysical Research Letters, 52, e2025GL114939.
(23)Wang, XY., Wang, X., Zhang, XC. et al. 2019. Creep damage characterization of UNS N10003 alloy based on a numerical simulation using the Norton creep law and Kachanov–Rabotnov creep damage model. NUCL SCI TECH 30, 65.
(24)D. Guner, H. Ozturk. 2019. Experimental and modelling study on nonlinear time-dependent behaviour of thin spray-on liner. Tunnelling and Underground Space Technology, 84, 306-316.
(25)Zheng, M., Han, L., Qiu, Z., et al. 2016. Simulation of permanent deformation in high-modulus asphalt pavement using the Bailey-Norton creep law. Journal of Materials in Civil Engineering, 28(7), 04016020.
(26)He, M.C., Li, C., Gong, W.L., et al. 2016. Support principles of NPR bolts/cables and control techniques of large deformation. Chin J Rock Mech Eng, 35(8): 1513–1529.
(27)Chen, F., Wang, Xb., Du, Yh. et al. 2021. Numerical analysis of the precursory information of slope instability process with constant resistance bolt. Sci Rep, 11, 21814.
(28)Wang, B., Zuo, Q., Deng, M. et al. 2025. Deformation Characteristics and Chain Mechanism of the Tanjiahe Landslide in the Three Gorges Reservoir Area Under the Synergistic Effect of Rainfall, Reservoir Water, and Groundwater. Rock Mech Rock Eng 58, 5235–5254.
(29)Preisig, G. , Eberhardt, E. , Smithyman, M. , Preh, A. & Bonzanigo, L. Hydromechanical rock mass fatigue in deep-seated landslides accompanying seasonal variations in pore pressures. Rock. Mech. Rock. Eng. 49, 2333– 2351 (2016).
(30)Cochran,E.S., Vidale,J. E.&Tanaka,S. 2004. Earth tides can trigger shallow thrust fault earthquakes. Science 306, 1164–1166.
(31)Bell, M. L. &Nur, A. 1978. Strength changes due to reservoir-induced pore pressure and stresses and application to Lake Oroville. J. Geophys. Res. Solid Earth 83, 4469–4483.
(32)Schultz, R., Atkinson, G., Eaton, D. W., et al. 2018. Hydraulic fracturing volume is associated with induced earthquake pro-ductivity in the Duvernay play. Science 359,304–308.

(33)Hill, R. G.,Weingarten, M., Rockwell, T. K., et al. 2023. Major southern San Andreas earthquakes modulated by lake-filling events. Nature, 618,761–766.
(34)Amos, C. B. et al. 2014. Uplift and seismicity driven by groundwater depletion in central California. Nature 509,483–486.
(35)Vasseur, J. et al. 2017. Does an inter-flaw length control the accuracy of rupture forecasting in geological materials?. Earth Planet. Sci. Lett. 475, 181–189.
(36)Patton, A., Goebel, T., Kwiatek, G., et al. 2023. Large-scale heterogeneities can alter the characteristics of compressive failure and accelerated seismic release. Phys. Rev. E 108, 014131.
(37)Goebel, T. H. W., Schuster, V., Kwiatek, G., et al. 2024. A laboratory perspective on accelerating preparatory processes before earthquakes and implications for foreshock detectability. Nat. Commun. 15, 5588.
(38)Ross, Z. E. et al. 2020. 3D fault architecture controls the dynamism of earthquake swarms. Science 368, 1357– 1361.
(39)Ellsworth, W. L. 2013. Injection-induced earthquakes. Science 341, 6142.
(40)Wei, S. et al. 2015. The 2012 Brawley swarm triggered by injection-induced aseismic slip. Earth Planet. Sci. Lett. 422, 115– 125.
(41)Pei, S., Niu, F., Ben-Zion, Y. et al. 2019. Seismic velocity reduction and accelerated recovery due to earthquakes on the Longmenshan fault. Nat. Geosci. 12, 387–392.
(42)Deshpande, N. S., Furbish, D. J., Arratia, P. E., et al. 2021. The perpetual fragility of creeping hillslopes. Nat. Commun. 12, 3909.
(43)Yuan, Y., Zeng, Z., Xing, Y. et al. 2024. From creep to flow: Granular materials under cyclic shear. Nat Commun 15, 3866.
(44)Riva, F., Agliardi, F., Amitrano, D., et al. 2018. Damage based time dependent modeling of paraglacial to postglacial progressive failure of large rock slopes. J. Geophys. Res.: Earth Surf. 123, 124–141.
(45)Furuki, H. & Chigira, M. 2019. Structural features and the evolutionary mechanisms of the basal shear zone of a rockslide. Eng. Geol. 260, 105214.
(46)Schäbitz, M. et al. 2018. Microstructures in landslides in northwest China— implications for creeping displacements? J. Struct. Geol. 106, 70–85.
(47)Kamb, B. et al. 1985. Glacier surge mechanism: 1982-1983 surge of variegated glacier, alaska. Science 227, 469–479.
(48)Jiskoot, H., Murray, T. & Boyle, P. 2000. Controls on the distribution of surge-type glaciers in Svalbard. J. Glaciol. 46, 412–422.
(49)Sevestre, Heïdi & Benn, D. I. 2015. Climatic and geometric controls on the global distribution of surge-type glaciers: implications for a unifying model of surging. J. Glaciol. 61, 646–662.
(50)Nanni, U., Bouchayer, C., Åkesson, H. et al. 2025. Observed positive feedback between surface ablation and crevasse formation drives glacier acceleration and potential surge. Nat Commun 16, 11227.

(51)Leinauer, J., Weber, S., Cicoira, A. et al. 2023. An approach for prospective forecasting of rock slope failure time. Commun Earth Environ 4, 253.
(52)Zhou, X.P., Liu, L.J., Xu, Ce. 2020. A modified inverse-velocity method for predicting the failure time of landslides, Engineering Geology, 268, 105521.
(53)Loew, S., Schneider, S., Josuran, M. et al. 2025. Early warning and dynamics of compound rockslides: lessons learnt from the Brienz/Brinzauls 2023 rockslope failure. Landslides, 22, 283-298.
(54). Hao, S., Liu, C., Lu, C. et al. 2016. A relation to predict the failure of materials and potential application to volcanic eruptions and landslides. Sci Rep 6, 27877.